



Multilayered density profile for noninteracting fermions in a rotating two-dimensional trap

Manas Kulkarni, Satya N. Majumdar, Grégory Schehr

► To cite this version:

Manas Kulkarni, Satya N. Majumdar, Grégory Schehr. Multilayered density profile for noninteracting fermions in a rotating two-dimensional trap. *Physical Review A*, 2021, 103 (3), 10.1103/PhysRevA.103.033321 . hal-03179775

HAL Id: hal-03179775

<https://hal.science/hal-03179775>

Submitted on 16 Dec 2023

HAL is a multi-disciplinary open access archive for the deposit and dissemination of scientific research documents, whether they are published or not. The documents may come from teaching and research institutions in France or abroad, or from public or private research centers.

L'archive ouverte pluridisciplinaire **HAL**, est destinée au dépôt et à la diffusion de documents scientifiques de niveau recherche, publiés ou non, émanant des établissements d'enseignement et de recherche français ou étrangers, des laboratoires publics ou privés.

Multilayered density profile for noninteracting fermions in a rotating two-dimensional trap

Manas Kulkarni,¹ Satya N. Majumdar,² and Grégory Schehr^{2,3}

¹*International Centre for Theoretical Sciences, Tata Institute of Fundamental Research, Bengaluru – 560089, India*

²*LPTMS, CNRS, Univ. Paris-Sud, Université Paris-Saclay, 91405 Orsay, France*

³*Sorbonne Université, Laboratoire de Physique Théorique et Hautes Energies,*

CNRS UMR 7589, 4 Place Jussieu, 75252 Paris Cedex 05, France

(Dated: Tuesday 28th December, 2021)

We compute exactly the average spatial density for N spinless noninteracting fermions in a 2d harmonic trap rotating with a constant frequency Ω in the presence of an additional repulsive central potential γ/r^2 . We find that, in the large N limit, the bulk density has a rich and nontrivial profile – with a hole at the center of the trap and surrounded by a multi-layered “wedding cake” structure. The number of layers depends on N and on the two parameters Ω and γ leading to a rich phase diagram. Zooming in on the edge of the k^{th} layer, we find that the edge density profile exhibits k kinks located at the zeroes of the k^{th} Hermite polynomial. Interestingly, in the large k limit, we show that the edge density profile approaches a limiting form, which resembles the shape of a propagating front, found in the unitary evolution of certain quantum spin chains. We also study how a newly formed droplet grows in size on top of the last layer as one changes the parameters.

I. INTRODUCTION

Noninteracting spinless fermions in a confining trap is a subject of much current theoretical and experimental interest [1–7]. On one hand, this system is realisable in cold atom experiments, and several techniques such as absorption imaging [8–10] for collective density measurements and quantum gas microscopes [11–13] for direct in situ imaging of the individual fermions with remarkably high resolutions are available. On the other hand, it is simple enough to be analytically tractable and yet exhibits rich and nontrivial spatial fluctuations, even at zero temperature, due to the Pauli exclusion principle [14–20]. While the bulk density is usually well described by the local density approximation (LDA) [8, 21], this approximation breaks down near the edges of the Fermi gas, induced by the trap. A number of recent studies have pointed out that LDA is not sufficient to capture the density fluctuations and correlations near the edges [15, 17–19, 22]. For certain one-dimensional trapping potentials, such as the harmonic trap, an exact mapping was found between the positions of the fermions in the ground state and the eigenvalues of a suitable random matrix ensemble [15, 16] – for a recent review see [23]. Using results from the random matrix theory (RMT), the density correlations near the edges were computed exactly and their universal properties (with respect to the shape of the trapping potential) were elucidated [15, 17–19, 24–28]. The connection to RMT does not hold generically in higher dimensions. However, using the determinantal properties of the noninteracting fermions, the edge properties in higher dimensions could still be computed analytically [18, 19].

A particularly interesting situation corresponds to fermions in a rotating trap in two-dimensions, which has been studied recently both experimentally [29–31] and theoretically [32–34]. In this system, the single particle

Hamiltonian, in the rotating frame, is given by [35, 36]

$$\hat{H} = \frac{p^2}{2m} + V(r) - \Omega L_z \quad (1)$$

where $V(r)$ is a confining central potential, $L_z = xp_y - yp_x = -i(x\partial_y - y\partial_x)$ is the z -component of the angular momentum and Ω is the rotation frequency. For the harmonic trap $V(r) = (1/2)m\omega^2 r^2$, an important parameter is the ratio $\nu = \Omega/\omega$, which must satisfy $0 < \nu < 1$ to keep the fermions confined. The limit $\nu \rightarrow 0$ corresponds to fermions in a non-rotating harmonic trap while in the opposite limit $\nu \rightarrow 1$, this problem can be mapped to the celebrated Landau problem of noninteracting fermions in a plane in the presence of a perpendicular magnetic field [37]. Interestingly, in this $\nu \rightarrow 1$ limit, the positions of N fermions in the ground state map onto the eigenvalues of the classical complex Ginibre ensemble of RMT [34], where one considers a random $N \times N$ matrix with independent complex Gaussian entries [38]. In this mapping, one assumes that the N fermions are confined in the lowest Landau level, which can be realized by setting $1 - 2/N < \nu < 1$. With this assumption, the bulk density for large N is rather simple: it is just uniform over the disk of radius \sqrt{N} centred at the origin [34].

This uniform bulk density emerges because, in the ground state, the fermions are all in the lowest Landau level. A natural question then is: how the density may change if the many-body ground state also contains single-particle states belonging to higher Landau levels? Indeed, this is a generic situation as one increases N , for fixed ν . In addition, since the potential $V(r)$ is radially symmetric, it is convenient to solve the corresponding Schrödinger equation in polar coordinates, which will automatically generate an effective repulsive interaction $\sim 1/r^2$ in the radial direction. Hence it is natural to consider a more generic potential from the start

$$V(r) = \frac{1}{2}m\omega^2 r^2 + \frac{\gamma}{2r^2}, \quad \gamma \geq 0. \quad (2)$$

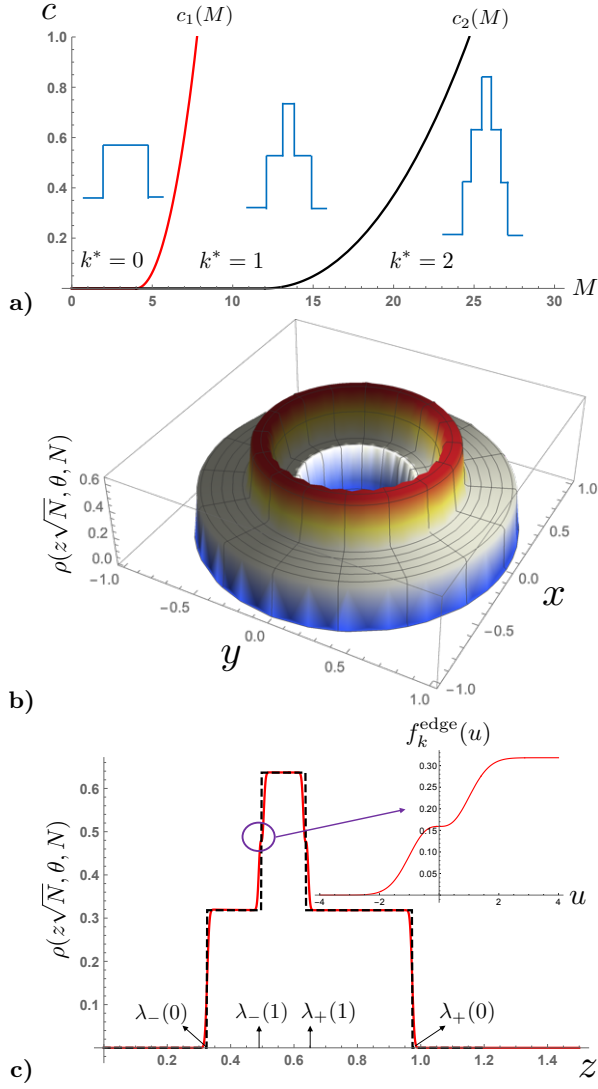


FIG. 1. **(a)**: Phase diagram in the (M, c) plane. It is divided into regions labeled by $k^* = 0, 1, 2, \dots$ denoting the number of bands (n) that are below the Fermi level. The lines $c_n(M)$ separates the regions between $k^* = n - 1$ and $k^* = n$. In each of the regions, a typical (representative) density profile is shown (blue). We see that every new band creates a new layer in the density. **(b)**: A 3D representation of the exact density in (6). A hole around the origin is surrounded by a multi-layered “wedding cake” structure. **(c)**: Plot showing the comparison between the exact density in (6) (red solid) and the large N asymptotic bulk density (10) (black dashed) for $c = 1$, $M = 10$ and $N = 8000$ (this corresponds to $k^* = 1$ in the phase diagram). We zoomed in on the left edge of the $k = 1$ layer and the inset shows the scaling function $f_1^{\text{edge}}(u)$ in (11) plotted vs u .

We thus have two parameters $0 < \nu < 1$ and $\gamma \geq 0$. In this paper we investigate the density profile in the ground state, for large N , as a function of ν and γ and find an extremely rich phase diagram in the (ν, γ) plane.

Let us first summarise our main results. We find that in the large N limit the appropriate rescaled parameters

are

$$c = \frac{\gamma}{N} \quad \text{and} \quad M = (1 - \nu^2) N, \quad (3)$$

which are both kept of order $O(1)$ as $N \rightarrow \infty$. We will show later that this scaling is necessary to keep the average density of fermions of order $O(1)$ as $N \rightarrow \infty$. The phase diagram in the (M, c) plane is depicted in Fig. 1 a). There are series of critical lines $c_1(M), c_2(M), \dots$ that separate the regions labelled by k^* where $k^* + 1$ is the number of Landau levels included in the ground state. As one crosses these critical lines, the density profile undergoes abrupt changes, as shown in Fig. 1 a). For a given k^* the bulk density vanishes for $r < \sqrt{l_-(0)}$ thus creating a hole around the origin [see Fig. 1 b)]. Outside the hole, the density is nonzero over an annulus $\sqrt{l_-(0)} < r < \sqrt{l_+(0)}$. On top of this annulus, there is a “wedding cake” structure [see Fig. 1 b)] with k^* layers with progressively smaller supports but with equal heights $1/\pi$. For example the k -th layer has support on $\sqrt{l_-(k)} < r < \sqrt{l_+(k)}$ (see Fig. 1). As shown later, $l_{\pm}(k) = O(N)$. We also investigated the change in the density profile as one crosses the critical lines in the phase diagram and found an interesting “travelling front structure” in the density. Furthermore, if we zoom in on the left boundary of the k -th layer (and symmetrically on the right boundary), i.e., close to $\sqrt{l_-(k)}$ (and symmetrically at $\sqrt{l_+(k)}$) we find a nontrivial edge-profile of the density (11) with k kinks whose locations coincide with the zeros of the k -th Hermite polynomial $H_k(-u) = 0$ with u denoting the scaled distance from $\sqrt{l_-(k)}$ (see inset of Fig. 1 (c)). Finally, in the limit where $k \gg 1$, the edge profile approaches a nontrivial limiting form, which we compute exactly. Interestingly, the same limiting form has appeared in completely different problems, such as in a propagating one-dimensional fermionic front separating a high and low density phases and evolving unitarily in time [39–43].

II. MODEL AND PROPERTIES

We start with the single particle Hamiltonian in (1) with $V(r)$ in Eq. (2). The model turns out to be integrable in the sense that the Schrödinger equation $\hat{H}\psi_{k,l}(r, \theta) = E_{k,l}\psi_{k,l}(r, \theta)$ is exactly solvable in the polar coordinates (see Appendix A for details). For convenience, we set $m = \hbar = 1$. We get

$$\psi_{k,l}(r, \theta) = a_{k,l} L_k^\lambda(r^2) r^\lambda e^{-r^2/2} e^{i l \theta}, \quad \text{with } \lambda = \sqrt{\gamma + l^2}, \quad (4)$$

where $L_k^\lambda(x)$ are the generalised Laguerre polynomials and the normalisation gives $a_{k,l}^2 = \frac{\Gamma(k+1)}{\pi \Gamma(k+1+\lambda)}$. The associated eigenvalues, in units of ω , are given by (see Appendix B for details)

$$E_{k,l} = 2k + 1 + \sqrt{\gamma + l^2} - \nu l. \quad (5)$$

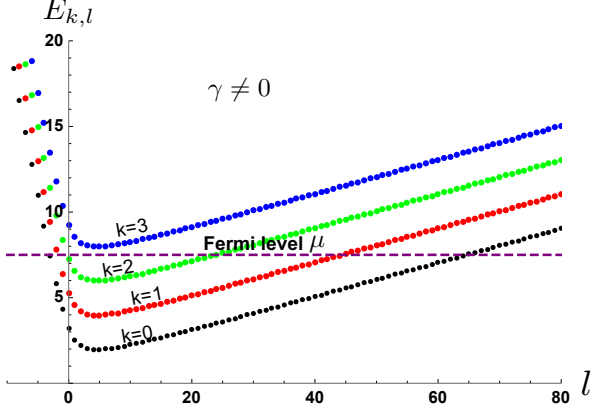


FIG. 2. Energy levels $E_{k,l}$ in (5) vs l for $k = 0, 1, 2, 3$, for $\gamma = 5$ and $\nu = 0.9$. The purple (dashed) horizontal line marks the Fermi level, $\mu = 7.5$. Only the states with energy below μ can contribute to the ground state.

The single particle states are labelled by a pair of integers (k, l) with $k = 0, 1, 2, \dots$ and $l = 0, \pm 1, \pm 2, \dots$. The energy levels (5) are shown in Fig. 2. Different values of k correspond to different bands or Landau levels.

We now consider N spinless noninteracting fermions in their ground state. The many-body ground-state is thus given by a Slater determinant constructed from N single particle eigenfunctions associated to the lowest N eigenvalues. For a given N , the eigenfunctions participating in the Slater determinant may belong to multiple bands of the spectrum in Fig. 2 with k^* denoting the label of the highest band which is at least partially filled. We also denote by μ the Fermi energy, i.e. the energy of the highest occupied single particle energy level. The Fermi energy μ can be tuned by varying N . As μ increases, one sees from Fig. 2, where μ is indicated by a horizontal line, that more and more states with energy levels below μ contribute to the ground state since k^* also increases.

The average number density, normalised to N , at a point $\mathbf{r} = (r, \theta)$ is given by $\rho(r, \theta, N) = \sum_{i=1}^N \langle \delta(\mathbf{r} - \mathbf{r}_i) \rangle$ where $\langle \dots \rangle$ denotes the expectation value in the ground state. For noninteracting fermions, it can be computed explicitly in terms of single particle eigenfunctions

$$\rho(r, \theta, N) = \sum_{k,l} |\psi_{k,l}(r, \theta)|^2 = \sum_{k=0}^{k^*} \rho_k(r, \theta, N), \quad (6)$$

where $\rho_k(r, \theta, N)$ denotes the density from the k^{th} band and is given by

$$\rho_k(r, \theta, N) = \frac{\Gamma(k+1) e^{-r^2}}{\pi} \sum_{l=l_-(k)}^{l_+(k)} \frac{[L_k^\lambda(r^2)]^2 r^{2\lambda}}{\Gamma(\lambda + k + 1)}. \quad (7)$$

Here, $l_{\pm}(k)$ are the locations where the Fermi level μ intersects the k^{th} band, i.e. $E_{k,l_{\pm}(k)} = \mu$. Solving this equation using (5) (shifting energy by 1, effectively ab-

sorbing it in μ) gives

$$l_{\pm}(k) = \frac{\nu(\mu - 2k) \pm \sqrt{(\mu - 2k)^2 - \gamma(1 - \nu^2)}}{1 - \nu^2}. \quad (8)$$

For a given k , $E_{k,l}$ (Eq. 5) has a minimum at $l = l^*$ where $l^* = \frac{\nu}{\sqrt{1-\nu^2}} \sqrt{\gamma}$. Note that l^* is independent of k and the energy of the k^{th} band at this minimum is given by $E_{k,l^*} = 2k + \sqrt{(1 - \nu^2)\gamma}$. If the Fermi level has to intersect at least one band, we must have $E_{0,l^*} < \mu$ which implies $\mu > \sqrt{(1 - \nu^2)\gamma}$. For a fixed μ , the number of bands k^* below μ can be obtained by simultaneously requiring $E_{k^*,l^*} = 2k^* + \sqrt{(1 - \nu^2)\gamma} < \mu$ and $E_{k^*+1,l^*} = 2k^* + 2 + \sqrt{(1 - \nu^2)\gamma} > \mu$ which yields $k^* = \text{Int} \left[\frac{\mu - \sqrt{(1 - \nu^2)\gamma}}{2} \right]$ where $\text{Int}(x)$ denotes the integer part of x (see Appendix B for details). The relation between the Fermi energy μ and N can be obtained by counting the total number of single particle levels with energy below μ . This gives $\sum_{k=0}^{k^*} [l_+(k) - l_-(k)] = N$ which fixes μ in terms of N (see Appendix B for details). For large N , it turns out that $\mu \sim O(1)$. So far, the results are exact for arbitrary N , $\nu \in (0, 1)$ and $\gamma > 0$. To make further progress we now work in the large N limit and re-scale the two parameters ν and γ as in Eq. (3). Thus c and M are the new rescaled parameters. It turns out that this scaling is necessary to keep $\rho(r, \theta, N) = O(1)$ for large N . In terms of c and M , we have from Eq. (8), $l_{\pm}(k) = \lambda_{\pm}(k)N$ where $\lambda_{\pm}(k) = \frac{(\mu - 2k) \pm \sqrt{(\mu - 2k)^2 - cM}}{M}$ and $k^* = \text{Int} \left[\frac{\mu - \sqrt{cM}}{2} \right]$.

III. CRITICAL LINES IN THE (M, c) PLANE

The (M, c) plane is divided into different regions labeled by $k^* = 0, 1, 2, \dots$ separated by critical lines [see Fig. 1 a)]. For there to be k^* bands, we require, $2k^* + \sqrt{cM} < \mu < 2(k^* + 1) + \sqrt{cM}$. Setting the upper bound, $\mu = 2(k^* + 1) + \sqrt{cM}$, one gets $\frac{4}{M} \sum_{q=1}^{k^*+1} \sqrt{q(q + \sqrt{cM})} = 1$ (see Appendix C for details). Solving this equation for c as a function of M gives the critical line $c_{k^*+1}(M)$. Thus, in the (M, c) plane, we get different regions labeled by $k^* = 0, 1, 2, \dots$. The region between $c_n(M)$ and $c_{n+1}(M)$ corresponds to the region with $k^* = n$, i.e. the Fermi level includes n bands below it. For instance, $c_1(M)$ and $c_2(M)$ can be explicitly computed (see Appendix C for details) and are plotted in Fig. 1 a), e.g., $c_1(M) = (1/M) (M^2/16 - 1)^2 \Theta(M - 4)$ where $\Theta(x)$ is the Heaviside step function.

IV. DENSITY IN THE LARGE- N LIMIT

We start by analysing the large N limit of $\rho_k(r, \theta, N)$ in Eq. (7) upon setting $r = z\sqrt{N}$. Since $l_{\pm}(k) = \lambda_{\pm}(k)N$, we can replace the discrete sum over l by an integral. We show (see Appendix D and E for details) that it converges to the following form

$$\rho_k(z\sqrt{N}, \theta, N) \approx \frac{2^{-k}}{\pi^{3/2} k!} \int_{a_-(k)}^{a_+(k)} dx e^{-x^2} [H_k(x)]^2 \quad (9)$$

where $a_{\pm}(k) = \frac{(\lambda_{\pm}(k) - z^2)\sqrt{N}}{z\sqrt{2}}$ and $H_k(x)$ is the k^{th} Hermite polynomial. For fixed z , as $N \rightarrow \infty$, the two bounds $a_+(k) \rightarrow \infty$ and $a_-(k) \rightarrow -\infty$ iff $\sqrt{\lambda_-(k)} < z < \sqrt{\lambda_+(k)}$. If z is outside this interval, both bounds tend to either $+\infty$ or $-\infty$ simultaneously. In the latter cases, the integral in (9) vanishes as $N \rightarrow \infty$. In contrast, in the former case, the integral approaches a finite value $\int_{-\infty}^{\infty} dx e^{-x^2} [H_k(x)]^2 = 2^k k! \sqrt{\pi}$. Hence we conclude that the density from the k^{th} band at a fixed rescaled distance $z = r/\sqrt{N}$ converges to

$$\rho_k^{\text{bulk}}(r, \theta, N) \approx \frac{1}{\pi} \mathcal{I}_{\sqrt{\lambda_-(k)} < z < \sqrt{\lambda_+(k)}}, \quad (10)$$

where the function \mathcal{I} takes value 1 if the inequality in the subscript is satisfied and 0 otherwise. Thus the bulk density is flat (with value $1/\pi$) inside the k^{th} annulus $\sqrt{\lambda_-(k)} < z < \sqrt{\lambda_+(k)}$ [see Fig. 1 b)]. We find in Fig. 1 c) an excellent agreement between the results obtained from the exact evaluation of the sum in (6) and (7) for $k^* = 1$ and the large N bulk density in Eq. (10). For a fixed $k^* \geq 1$, the sum in Eq. (6) gives a superposition of contributions of the type (10) for each $k \leq k^*$, leading to the “wedding cake” structure in Fig. 1 b).

If z is close to one of the two edges, say the left edge $\sqrt{\lambda_-(k)}$, we can estimate the limiting form of the edge density when $N \rightarrow \infty$ from the same Eq. (9). For this, we set $z^2 = \lambda_-(k) + \frac{\sqrt{2\lambda_-(k)}}{\sqrt{N}}u$ where $u \sim O(1)$. In this case, the lower limit in the integral in Eq. (9) becomes $a_-(k) \approx -u$ (with u measuring the scaled distance from the left edge), while the upper limit still approaches to $+\infty$ as $N \rightarrow \infty$. Hence, we get,

$$\rho_k^{\text{edge}}(r, \theta, N) \approx f_k^{\text{edge}}(u) \quad (11)$$

where $f_k^{\text{edge}}(u) = \frac{2^{-k}}{\pi^{3/2} k!} \int_{-u}^{\infty} dx e^{-x^2} [H_k(x)]^2$. Note that when $u \rightarrow \infty$, $f_k^{\text{edge}}(u) \rightarrow 1/\pi$, and the edge density matches smoothly with the bulk density. In Fig. 1 we have zoomed in on the left edge of $k = 1$ layer and plotted the scaling function $f_1^{\text{edge}}(u)$ in the inset, which clearly shows a kink where $df_1^{\text{edge}}/du = 0$. For the k^{th} layer, setting $df_k^{\text{edge}}(u)/du = 0$ (which implies $H_k(-u) = 0$), it follows that there will be k kinks in $f_k^{\text{edge}}(u)$ whose locations coincide with the k zeros of $H_k(-u)$. The scaling function $f_k^{\text{edge}}(u)$ is actually universal in the sense that

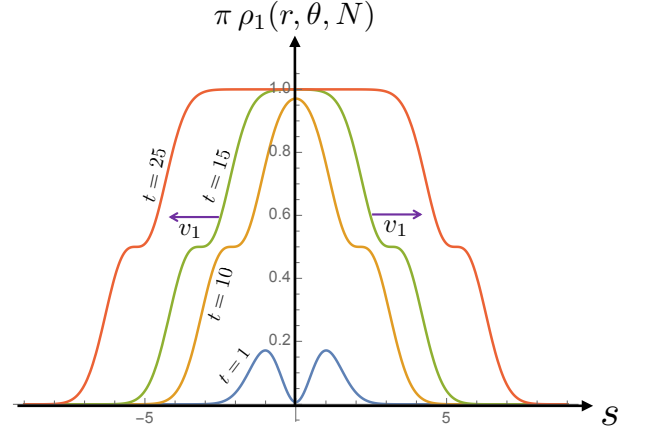


FIG. 3. Density profile in Eq. (14) for $M = 5$ plotted as a function of the scaled distance s [49] for increasing values of $t = 1, 10, 15$ and 25 . As t increases, the scaled density approaches the constant value $1/\pi$ for $|s| < v_1 t$ and decays rapidly to 0 for $|s| > v_1 t$. For $t \gg 1$, the forward and backward fronts separating the constant density $1/\pi$ and the zero-density outside move ballistically in opposite directions with a constant speed v_1 .

it does not depend on c and M explicitly. In fact, in the special case $\gamma = 0$ and $\nu = 1$, but with fixed N (the classical Landau problem) – hence not in the scaling limit discussed here –, the edge density ρ_k for the k^{th} Landau level was studied in [45] and similar kinks were found for finite N , but the scaling function $f_k^{\text{edge}}(u)$ was not computed (see also [46] in the mathematics literature in the context of polyanalytic Ginibre ensembles).

Furthermore, an interesting limiting shape emerges for $f_k^{\text{edge}}(u)$ in the scaling limit of k large and u large but with the ratio $y = u/\sqrt{2k}$ fixed. In this case, we find (see Appendix E for details)

$$\lim_{k \rightarrow \infty} f_k^{\text{edge}}(\sqrt{2k}y) = \frac{1}{\pi^2} \cos^{-1}(-y) \mathcal{I}_{-1 < y < 1}, \quad (12)$$

and for $y > 1$ it takes a value of $1/\pi$. Interestingly, a similar shape appeared in the description of a propagating front in the quantum evolution of a spin chain (equivalent to free fermions on a lattice) [39–43]. It turns out that there is yet another interesting scaling regime close to the two endpoints $u \approx \pm\sqrt{2k}$. For example, setting $u = -\sqrt{2k} + \frac{w}{\sqrt{2k^{1/6}}}$ with $w = O(1)$

$$\lim_{k \rightarrow \infty} k^{1/3} \pi f_k^{\text{edge}}\left(-\sqrt{2k} + \frac{w}{\sqrt{2k^{1/6}}}\right) = \mathcal{F}(w) \quad (13)$$

where $\mathcal{F}(w) = ([\text{Ai}'(-w)]^2 + w \text{Ai}^2(-w))$ where $\text{Ai}(z)$ denotes the Airy function. Interestingly, the same scaling function describes the tail of the density of eigenvalues (centered and scaled) in the Gaussian Unitary Ensemble of RMT [47, 48].

V. CROSSING THE CRITICAL LINE IN THE (M, c) PLANE

When k^* changes from $k^* = 0$ to $k^* = 1$ (which means a new band is included below the Fermi level), one may wonder how the density profile changes from a one-layered structure to a two-layered structure. When one crosses this critical line $c = c_1(M) \equiv c_1$, the second layer appears on top of the first layer (Fig. 1). Here, we describe the evolution of the density profile of this newly formed droplet as a function of the distance $c_1 - c$ below the critical line c_1 for fixed $4 < M < 12$ (see Appendix F for details). As k^* changes from 0 to 1, the Fermi level μ exceeds the value $\mu = 2 + \sqrt{c_1 M}$ by a small amount δ : $\mu = 2 + \sqrt{c_1 M} + \delta$ where $\delta \ll 1$. As k^* jumps from 0 to 1, we find that the additional macroscopic density in the second layer appears over the scaled region $\sqrt{\frac{c_1}{M}} - v_1 \sqrt{\delta} < z^2 < \sqrt{\frac{c_1}{M}} + v_1 \sqrt{\delta}$ where $v_1 = \frac{\sqrt{2}}{M}(c_1 M)^{1/4}$ and $z = r/\sqrt{N}$. Therefore, the center of the second layer appears at $z_c = (c_1/M)^{1/4}$. Here, we give a scaling description of this density in the second layer just after its appearance, i.e., in the limit $\delta \rightarrow 0$. Let $z^2 = \sqrt{\frac{c_1}{M}} + \epsilon$, where ϵ measures the distance from the center of the second layer. We analyse Eq. (7) with $k = 1$ by replacing, for large N , the sum by an integral and evaluating it by the saddle point method (see Appendix F for details). This leads to the following density profile of the droplet (for a plot see Fig. 3)

$$\rho_1(z\sqrt{N}, \theta, N) \approx \frac{1}{\pi} [F_1(s + v_1 t) - F_1(s - v_1 t)] \quad (14)$$

where $F_1(z) = \frac{1}{2} \left[\text{erfc}(z) - \frac{2}{\sqrt{\pi}} z e^{-z^2} \right]$ with $\text{erfc}(z)$ being the complementary error function. Here $s = \epsilon \sqrt{N/2}(M/c_1)^{1/4}$ is the scaled distance measured from the center of the droplet, while $t = \sqrt{N/2}(M/c_1)^{1/4} \sqrt{\delta}$ is proportional to $c_1 - c > 0$, measuring the deviation from the critical line. If we interpret s and t as space and time, the density profile in Eq. (14) has an interesting interpretation: the two edges of this profile move ballistically away from the droplet center with a constant speed v_1 . At large t , the widths of these “solitonic” fronts remain of $O(1)$ while the height of the density behind the fronts approaches a constant value $1/\pi$ (see Fig. 3). This picture can be easily generalized to other critical lines in the (M, c) plane (see Appendix F for details).

VI. CONCLUSIONS

To conclude, we have shown analytically that the average density profile in the ground-state of N *noninteracting* fermions in a rotating trap exhibits a rich multi-layered “wedding cake” structure, as more and more Landau levels participate in the ground state by increasing N , leading to a highly interesting phase diagram in the parameter space. This non-trivial density profile owes

its origin entirely to quantum effects, and can not be obtained from a simple Local Density/Thomas-Fermi approximation. It would be interesting to study the effect of the inclusion of more and more Landau levels on other observables, going beyond the one-point function studied in this paper, such as the number variance and the entanglement entropy (see for e.g., [34, 50–52]). We note that strongly interacting bosons and fermions have been studied experimentally in rotating traps leading in particular to the formation of vortex lattices [53, 54]. In our case, there is a hole in the density at the center of the trap, but this is due to the repulsive inverse square interaction $\gamma/(2r^2)$ and it is not related to a vortex. It will be challenging to see how interactions can change the above scenario, in particular leading to the generation of vortices.

ACKNOWLEDGMENTS

We thank Gautam Mandal and Takeshi Morita for very useful discussions at the initial stage of this work. MK acknowledges support from the project 6004-1 of the Indo-French Centre for the Promotion of Advanced Research (IFCPAR), Ramanujan Fellowship (SB/S2/RJN-114/2016), SERB Early Career Research Award (ECR/2018/002085) and SERB Matrices Grant (MTR/2019/001101) from the Science and Engineering Research Board (SERB), Department of Science and Technology, Government of India. MK thanks the hospitality of Laboratoire de Physique, Ecole Normale Supérieure (Paris). This research was supported by ANR grant ANR-17-CE30-0027-01 RaMaTraF. MK acknowledges support of the Department of Atomic Energy, Government of India, under project no. RTI4001.

Appendix A: Model and basic properties

As mentioned in the main text, our starting Hamiltonian is,

$$\hat{H} = \frac{p^2}{2} + \frac{1}{2} \omega^2 r^2 + \frac{\gamma}{2r^2} - \Omega L_z \quad (A1)$$

where $L_z = xp_y - yp_x = -i(x\partial_y - y\partial_x)$ is the z -component of the angular momentum, γ characterises the repulsive-like potential at the centre (inverse-square type), ω is the trap frequency and Ω is frequency at which the trap rotates around the vertical axis. For convenience, we have set the mass $m = 1$ and also $\hbar = 1$. Throughout the work, we will consider the case in which the inverse square central potential is very large, i.e.,

$$\gamma = cN, \quad c \sim O(1), \quad \text{regime of interest} \quad (A2)$$

In polar coordinates (r, θ) , the Hamiltonian reads,

$$\hat{H} = -\frac{1}{2} \left(\partial_r^2 + \frac{1}{r} \partial_r \right) + \frac{p_\theta^2}{2\hat{r}^2} + \frac{1}{2} \omega^2 \hat{r}^2 + \frac{\gamma}{2\hat{r}^2} - \Omega L_z \quad (\text{A3})$$

where

$$L_z = p_\theta = -i\partial_\theta \quad (\text{A4})$$

The first goal is to find eigenstates and eigenvalues of Eq. A3. Let us substitute,

$$\psi(r, \theta) = \psi(r) e^{il\theta} \quad (\text{A5})$$

where $l = 0, \pm 1, \pm 2, \dots$ are integers because the wave function needs to respect 2π periodicity in the angular direction. Then, we get,

$$\hat{H}\psi(r) = \left[-\frac{1}{2} \left(\partial_r^2 + \frac{1}{r} \partial_r \right) + \frac{1}{2} \omega^2 r^2 + \frac{\gamma + l^2}{2r^2} - l\Omega \right] \psi(r) \quad (\text{A6})$$

Hence, the equation we need to solve is, $\hat{H}\psi(r) = E\psi(r)$ which gives us,

$$\left[-\frac{1}{2} \left(\partial_r^2 + \frac{1}{r} \partial_r \right) + \frac{1}{2} \omega^2 r^2 + \frac{\gamma + l^2}{2r^2} - l\Omega \right] \psi(r) = E\psi(r) \quad (\text{A7})$$

To reduce the above eigenvalue equation (Eq. A7) to a standard form, we make the following transformation

$$\psi(r) = e^{-\omega r^2/2} r^{\sqrt{\gamma+l^2}} G(\omega r^2). \quad (\text{A8})$$

It is then easy to see that $G(z)$ satisfies the differential equation

$$zG''(z) + (b-z)G'(z) - aG(z) = 0, \quad (\text{A9})$$

$$\text{where} \quad \begin{cases} a = \frac{1}{2} \left[1 + \sqrt{\gamma + l^2} - \frac{E + \Omega l}{\omega} \right], \\ b = 1 + \sqrt{\gamma + l^2}. \end{cases} \quad (\text{A10})$$

This is a standard confluent hypergeometric differential equation whose general solution is given by the linear combination of two independent solutions as follows [55]

$$G(z) = A_1 z^{1-b} M(a-b+1, 2-b, z) + A_2 M(a, b, z) \quad (\text{A11})$$

where A_1 and A_2 are two arbitrary constants and

$$M(a, b, z) = \sum_{p=0}^{\infty} \frac{(a)_p}{(b)_p} \frac{z^p}{p!} = 1 + \frac{a}{b} z + \frac{a(a+1)}{b(b+1)} \frac{z^2}{2!} + \dots \quad (\text{A12})$$

is the Kummer's confluent hypergeometric function. Here, $(a)_p, (b)_p$ are Pochhammer symbols, i.e., $(a)_p = \frac{\Gamma(a+p)}{\Gamma(a)}$ where $\Gamma(x)$ is a Gamma function. Note that the arguments of the two functions in (A11) are different. The function $M(a, b, z)$ has the following asymptotic behaviors

$$M(a, b, z) \approx \begin{cases} 1 + \frac{a}{b} z + O(z^2), & z \rightarrow 0 \\ \frac{e^z z^{a-b}}{\Gamma(a)}, & z \rightarrow \infty. \end{cases} \quad (\text{A13})$$

Hence the most general solution for the eigenfunction $\psi(r)$ in Eq. A8 reads

$$\psi(r) = e^{-\omega r^2/2} r^{\sqrt{\gamma+l^2}} \times [A_1 (\omega r^2)^{1-b} M(a-b+1, 2-b, \omega r^2) + A_2 M(a, b, \omega r^2)], \quad (\text{A14})$$

where a and b are given in Eq. A10.

To fix these unknown constants A_1 and A_2 , we first consider the behavior of $\psi(r)$ as $r \rightarrow 0$. Using Eq. A13 we see that, as $r \rightarrow 0$, $\psi(r) \sim A_1 \omega^{-\sqrt{\gamma+l^2}} r^{-\sqrt{\gamma+l^2}}$. However, the eigenfunction must be square-integrable, i.e., $2\pi \int_0^\infty \psi^2(r) r dr$ should be finite. Substituting the small r behavior, we see that the integral behaves as $r^{2(1-\sqrt{\gamma+l^2})}$ in the lower limit $r \rightarrow 0$. Hence, since $l = 0, \pm 1, \dots$, the integral is divergent for all $\gamma > 1$. And this is indeed the case in our problem where γ is scaled as $\gamma = cN$ where $c = O(1)$ and $N \rightarrow \infty$ (see Eq. A2). Hence we must have $A_1 = 0$. Therefore the solution now reads

$$\psi(r) = A_2 e^{-\omega r^2/2} r^{\sqrt{\gamma+l^2}} M(a, b, \omega r^2). \quad (\text{A15})$$

We now consider the other limit $r \rightarrow \infty$. Substituting the asymptotic behaviour given in Eq. A13 in Eq. A15, we find that

$$\psi(r) \approx \frac{A_2}{\Gamma(a)} \omega^{a-b} r^{2a-b-1} e^{\omega r^2/2}. \quad (\text{A16})$$

Clearly, the integral $2\pi \int_0^\infty \psi^2(r) r dr$ diverges at the upper limit $r \rightarrow \infty$, provided $\Gamma(a)$ is finite. Hence, to cure this divergence, we must choose $|\Gamma(a)| = +\infty$, which means that $a = -k$ where $k = 0, 1, 2, \dots$ is a non-negative integer. In fact, this is the quantisation condition. In fact, when $a = -k$ the function $M(a = -k, b, z)$ is a polynomial of degree k and the wave function is square integrable. The quantisation condition $a = -k$, using Eq. A10, reads

$$\frac{\sqrt{\gamma+l^2}}{2} - \frac{l\Omega}{2\omega} - \frac{E}{2\omega} + \frac{1}{2} = -k. \quad (\text{A17})$$

The normalization condition fixes the constant $A_2 = c_{k,l}$, which depends on both quantum numbers k and l . Hence,

summarising, the complete set of eigenfunctions are given by

$$\psi_{k,l}(r, \theta) = c_{k,l} r^\lambda e^{-\omega r^2/2} M(-k, 1 + \lambda, \omega r^2) e^{il\theta}, \quad (\text{A18})$$

where $\lambda = \sqrt{\gamma + l^2}$ with the associated eigenvalues from Eq. A17

$$E_{k,l} = \omega[2k + 1 + \sqrt{\gamma + l^2}] - \Omega l. \quad (\text{A19})$$

Without loss of generality, we will set $\omega = 1$ (i.e., the energies are expressed in units of ω) and introduce $\nu \equiv \Omega/\omega < 1$. Note also that Kummer's confluent hypergeometric function are related to generalized Laguerre polynomials as,

$$M(-k, 1 + \lambda, r^2) = \frac{\Gamma(k+1)\Gamma(1+\lambda)}{\Gamma(1+k+\lambda)} L_k^\lambda(r^2). \quad (\text{A20})$$

Therefore, expressing Eq. A18 in terms of generalized Laguerre polynomials is preferable since these functions have an orthonormality condition that turns out to be useful

$$\int_0^\infty dx x^\lambda e^{-x} L_k^\lambda(x) L_{k'}^\lambda(x) dx = \frac{\Gamma(k+\lambda+1)}{\Gamma(k+1)} \delta_{kk'}. \quad (\text{A21})$$

The normalisation requirement $2\pi \int_0^\infty r dr |\psi_{k,l}(r)|^2 = 1$ finally gives,

$$\psi_{k,l}(r, \theta) = a_{k,l} L_k^\lambda(r^2) r^\lambda e^{-r^2/2} e^{il\theta} \quad (\text{A22})$$

with

$$a_{k,l}^2 = \frac{\Gamma(k+1)}{\pi \Gamma(k+1+\lambda)} \quad (\text{A23})$$

The associated eigenvalues are now expressed as,

$$E_{k,l} = 2k + 1 + \sqrt{\gamma + l^2} - \nu l \quad (\text{A24})$$

Eq. A22 and Eq. A24 form the complete solution of our system. In what follows, we will analyse the energy levels (Eq. A24) of the system.

Appendix B: Analysis of energy levels and the ground state

In this section, we will analyse the energy levels (Eq. A19) and discuss the ground state for a system which has N fermions. To start with, let us recap the $\gamma = 0$ case.

1. $\gamma = 0$ case

For $\gamma = 0$, Eq. A1 reduces to the Hamiltonian considered in Refs. [29, 30, 34]. The corresponding eigenfunctions were computed not in the polar coordinates,

rather in the coordinates (z, \bar{z}) where $z = x + iy$. In this representation, the eigenfunctions read (see e.g. Refs. [29, 30, 34, 50])

$$\psi_{n_1, n_2}(z, \bar{z}) = A_{n_1, n_2} e^{z\bar{z}/2} \partial_{\bar{z}}^{n_1} \partial_z^{n_2} e^{-z\bar{z}}, \quad (\text{B1})$$

with the associated eigenvalues (in units such that $\omega = 1$)

$$E_{n_1, n_2} = 1 + (1 - \nu)n_1 + (1 + \nu)n_2. \quad (\text{B2})$$

where $n_1 = 0, 1, 2, \dots$ and similarly $n_2 = 0, 1, 2, \dots$ where $0 < \nu = \Omega/\omega \leq 1$. This last condition follows from the fact that for $\nu > 1$, the system is “unstable” in the sense that the fermions can “fly away”. Another important point one can observe is that if $\omega = \Omega$, then it becomes the Landau problem (free electrons in perpendicular magnetic field) with energy levels given by,

$$E_{n_1, n_2}^{\text{Landau}} = 1 + 2\Omega n_2, \text{ Landau problem} \quad (\text{B3})$$

The lowest Landau level (LLL) is given by $n_2 = 0$. For a given n_2 , there is a N -fold degeneracy. We do not want degeneracy and therefore it can be lifted by choosing $\Omega < \omega$. This problem can also be alternatively solved in the polar coordinates discussed in the previous section. To see the connection between these two representations, we put $\gamma = 0$ in Eq. A19 and get

$$E_{k,l} = (2k + 1 + |l|) - \nu l \quad (\text{B4})$$

where, $k = 0, 1, 2, \dots$ and $l = 0, \pm 1, \pm 2, \dots$. Comparing Eq. B4 and Eq. B2, we get,

$$n_1 - n_2 = l, \quad n_1 + n_2 = 2k + |l| \quad (\text{B5})$$

which implies,

$$n_1 = k + \frac{l + |l|}{2}, \quad n_2 = k + \frac{|l| - l}{2}. \quad (\text{B6})$$

Therefore the LLL $n_2 = 0$ and $n_1 = 0, 1, 2, \dots$ corresponds to $k = 0, l = 0, 1, 2, \dots$. Note that, when $k = 0$, we have two branches (positive and negative l),

$$E_{k=0,l} = (1 + |l|) - \nu l \quad (\text{B7})$$

thus the LLL ($n_2 = 0$ and $n_1 = 0, 1, 2, \dots$) corresponds to the right branch ($l \geq 0$) and $k = 0$ in the polar representation of the eigenfunctions. The left panel of Fig. 5 shows the energy levels for the case of $\gamma = 0$.

2. $\gamma \neq 0$ case assuming $\gamma = cN$ where $c \sim O(1)$

Now, we discuss the case with $\gamma \neq 0$. This case turns out to be quite non-trivial. We recap that the energy levels are given by (Eq. A19),

$$E_{k,l} = 2k + 1 + \sqrt{\gamma + l^2} - \nu l \quad (\text{B8})$$

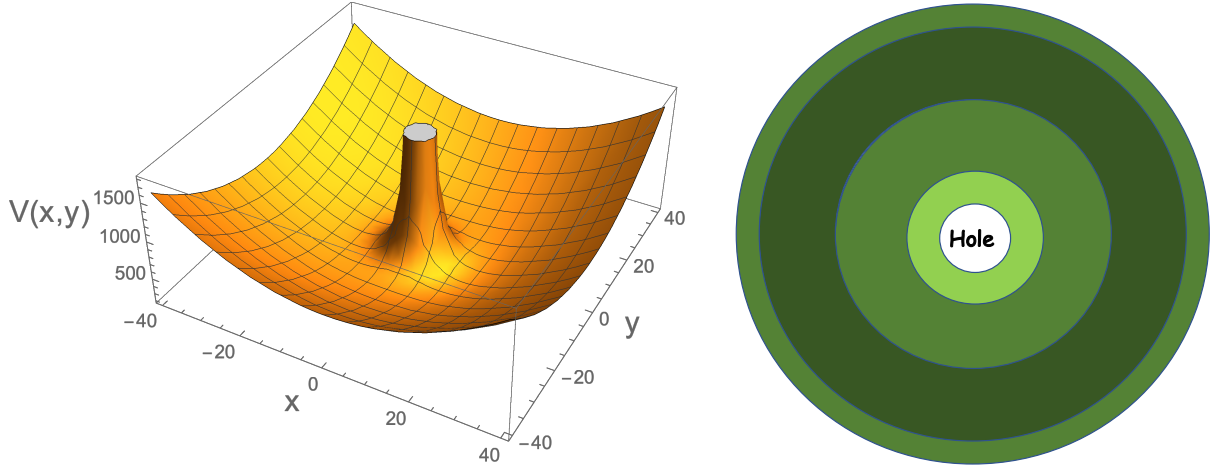


FIG. 4. (Left) The external potential $V(r) = \frac{1}{2}\omega^2 r^2 + \frac{\gamma}{2r^2}$ from Eq. A1 is plotted for visualization purposes. We took $c = 100$ and $N = 400$. We see the highly repulsive central potential that eventually causes a hole/empty region. (Right) Here, we show a schematic figure (top view) showing the fermions in 2D. The formation of the central hole and multiple layers and multiple edges is the key finding and property of the underlying Hamiltonian (Eq. A1). This is certainly missed via a traditional Local Density Approximation (see also Fig. 7).

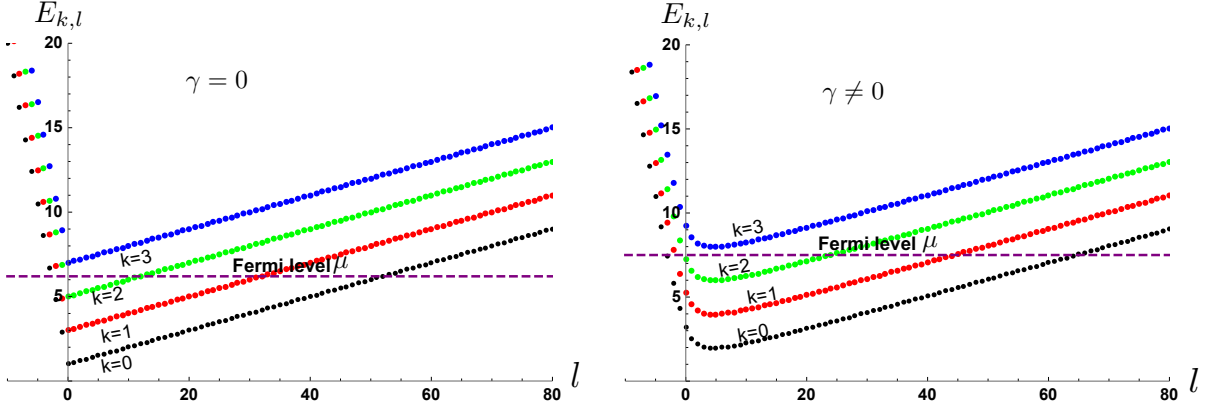


FIG. 5. (Left) Energy levels for the case $\gamma = 0$, $\nu = 0.9$ and $\mu = 6.2$ (Eq. A24). (Right) Energy levels for the case $\gamma = 5$, $\nu = 0.9$ and $\mu = 7.5$ (Eq. A24). For both figures, the purple (dashed) line shows the Fermi level upto which we are allowed to fill fermions. The black, red, green and blue curves represent $k = 0, 1, 2, 3$ bands respectively. The figures shows that if one fixes the Fermi level appropriately, then only three energy bands ($k = 0, 1, 2$) play a role. Instead of fixing the Fermi level, one can alternatively fix the number of Fermions N . These figures demonstrate the dramatic difference between $\gamma = 0$ and $\gamma \neq 0$ case.

For a given k , $E_{k,l}$ (Eq. B8, with energy shifted by 1 for convinience) has a minimum at $l = l^*$ where,

$$l^* = \frac{\nu}{\sqrt{1-\nu^2}} \sqrt{\gamma} \quad (\text{B9})$$

Note that l^* is independent of k and the energy of the k^{th} band at this minimum is given by,

$$E_{k,l^*} = 2k + \sqrt{(1-\nu^2)\gamma}. \quad (\text{B10})$$

We fix the Fermi level at μ . By varying μ , we can intersect the energy spectrum $E_{k,l}$ at different points. As μ increases, more and more k -bands of the spectrum become lower than the Fermi level and hence should be included in the construction of the many-body ground-state. The

right panel of Fig. 5 shows the energy levels for the case of $\gamma \neq 0$. It intersects the k^{th} band at two points $l_{\pm}(k)$ along the l -axis which can be easily computed by setting $E_{k,l} = \mu$ and we get,

$$l_{\pm}(k) = \frac{\nu(\mu - 2k) \pm \sqrt{(\mu - 2k)^2 - \gamma(1 - \nu^2)}}{1 - \nu^2}. \quad (\text{B11})$$

Note that if the Fermi surface has to intersect at least one band, we must have $E_{0,l^*} < \mu$ which indicates that,

$$\mu > \sqrt{(1-\nu^2)\gamma}. \quad (\text{B12})$$

For a fixed μ , the number of bands $k^* + 1$ below μ can

be obtained by setting,

$$\begin{aligned} E_{k^*, l^*} &= 2k^* + \sqrt{(1-\nu^2)\gamma} < \mu \\ E_{k^*+1, l^*} &= 2k^* + 2 + \sqrt{(1-\nu^2)\gamma} > \mu \end{aligned} \quad (\text{B13})$$

Hence k^* is given by,

$$k^* = \text{Int} \left[\frac{\mu - \sqrt{(1-\nu^2)\gamma}}{2} \right], \quad (\text{B14})$$

where $\text{Int}(x)$ denotes the integer part of x . Finally, the relation between the Fermi energy μ and N can be obtained by counting the total number of single particle levels with energy below μ . This gives,

$$\sum_{k=0}^{k^*} [l_+(k) - l_-(k)] = N. \quad (\text{B15})$$

Using Eq. B11, this gives,

$$\frac{2}{1-\nu^2} \sum_{k=0}^{k^*} \sqrt{(\mu - 2k)^2 - \gamma(1-\nu^2)} = N. \quad (\text{B16})$$

It is important to note that all the above results until now are valid for arbitrary N , arbitrary parameters $\nu \in [0, 1]$ and $\gamma > 0$.

We will now work in the large N limit, and set,

$$\gamma = cN, \quad (1-\nu^2)N = M, \quad \text{Large-}N \text{ limit} \quad (\text{B17})$$

Note that we are taking the limit $\nu \rightarrow 1$, $N \rightarrow \infty$, keeping $(1-\nu^2)N = M$ fixed. Therefore we have just two parameters c and M left and we want to calculate the average density in the ground state in the limit of large N , for fixed c and M . We will see that in the (M, c) plane, there is a series of critical lines separating phases with different density profiles. In terms of c and M we thus have

$$l_{\pm}(k) = \lambda_{\pm}(k)N, \quad (\text{B18})$$

where

$$\begin{aligned} \lambda_{\pm}(k) &= \frac{(\mu - 2k) \pm \sqrt{(\mu - 2k)^2 - cM}}{M}, \\ k^* &= \text{Int} \left[\frac{\mu - \sqrt{cM}}{2} \right]. \end{aligned} \quad (\text{B19})$$

Similarly the relation between μ and N in Eq. B16 becomes

$$\frac{2}{M} \sum_{k=0}^{k^*} \sqrt{(\mu - 2k)^2 - cM} = 1. \quad (\text{B20})$$

For fixed c and M , we have $\mu \sim O(1)$. Note that if we need $\lambda_{\pm}(k)$ in Eq. B18 to be $O(1)$, then we had to choose the scaling $\gamma = cN$. This justifies a posteriori the scaling $\gamma = cN$ for large N used in Eq. B17. Next, we will discuss this (M, c) plane and critical lines in this plane.

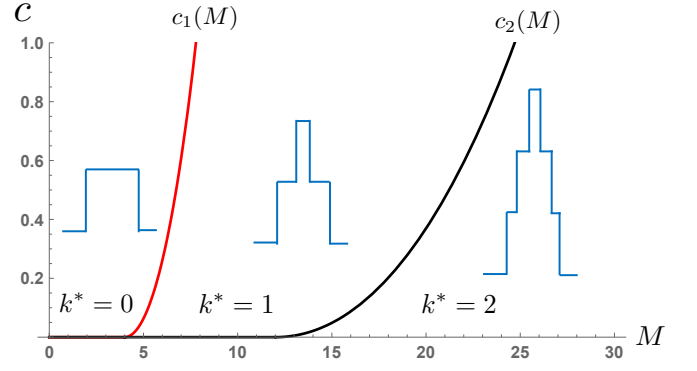


FIG. 6. Phase diagram in the (M, c) plane. It is divided into regions labeled by $k^* = 0, 1, 2, \dots$ denoting the number of bands (n) that are below the Fermi level. The lines $c_n(M)$ separates the regions between $k^* = n-1$ and $k^* = n$. In each of the regions, a typical (representative) density profile is shown (blue). We see that every new band creates a new layer in the density.

Appendix C: (M, c) plane and critical lines

The (M, c) plane gets divided in different regions, each labeled by $k^* = 0, 1, 2, \dots$. For example, if $k^* = 0$ (only the first band $k = 0$ is included in the ground state), we must have

$$\sqrt{cM} < \mu < 2 + \sqrt{cM}. \quad (\text{C1})$$

The upper inequality gets violated when $\mu = 2 + \sqrt{cM}$. Substituting this value of μ in Eq. B20 with $k^* = 0$, we get the first critical line $c = c_1(M)$ in the (M, c) plane [see Fig. 6],

$$c_1(M) = \begin{cases} \frac{1}{M} \left(\frac{M^2}{16} - 1 \right)^2, & M \geq 4 \\ 0 & M < 4. \end{cases} \quad (\text{C2})$$

Hence if $c \geq c_1(M)$, the ground state contains only the $k = 0$ band (i.e. $k^* = 0$).

Next, let us consider the case $k^* = 1$, i.e. two bands $k = 0$ and $k = 1$ are below the Fermi level μ . From the equation for k^* in Eq. B18 we see that $k^* = \text{Int}(\frac{\mu - \sqrt{cM}}{2}) = 1$ implies

$$2 + \sqrt{cM} < \mu < 4 + \sqrt{cM}. \quad (\text{C3})$$

The lower limit corresponds to the critical line $c = c_1(M)$ discussed before. The upper limit gives a new critical line $c = c_2(M)$ obtained by substituting $\mu = 4 + \sqrt{cM}$ in Eq. B20 with $k^* = 1$, i.e.,

$$\frac{2}{M} \left[\sqrt{(4 + \sqrt{cM})^2 - cM} + \sqrt{(2 + \sqrt{cM})^2 - cM} \right] = 1 \quad (\text{C4})$$

Solving for $c = c_2(M)$ we get,

$$c_2(M) = \begin{cases} \frac{17M^5 - 416M^3 - 12\sqrt{2}\sqrt{M^{10} - 48M^8 + 768M^6 - 4096M^4} + 2304M}{256M^2}, & M > 12 \\ 0, & 4 < M < 12 \end{cases} \quad (C5)$$

This second critical line (Eq. C5) is also plotted in Fig. 6. For higher values of k^* , one can obtain a similar formula for the critical line. For general k^* , the condition $k^* = \text{Int}(\frac{\mu - \sqrt{cM}}{2})$ indicates that,

$$2k^* + \sqrt{cM} < \mu < 2(k^* + 1) + \sqrt{cM}. \quad (C6)$$

Setting $\mu = 2(k^* + 1) + \sqrt{cM}$ in Eq. B20 and simplifying, one gets,

$$\frac{4}{M} \sum_{q=1}^{k^*+1} \sqrt{q(q + \sqrt{cM})} = 1. \quad (C7)$$

Solving this equation for c as a function of M gives the critical line $c_{k^*+1}(M)$. For $k^* = 0$ and $k^* = 1$ the explicit solutions are given respectively in Eqs. C2 and C5. However, one can easily work out the asymptotics. For example the line $c_{k^*+1}(M)$ starts from $M^* = 2(k^* + 1)(k^* + 2)$. For $k^* = 0$ and $k^* = 1$, this gives $M^* = 4$ and $M^* = 12$ respectively. For large M , it is easy to show from Eq. C7 that,

$$c_{k^*+1}(M) \approx \frac{M^3}{2^8 \left[\sum_{q=1}^{k^*+1} \sqrt{q} \right]^4}. \quad (C8)$$

Thus in the (M, c) plane, we get different regions labeled by $k^* = 0, 1, \dots$. The region between $c_n(M)$ and $c_{n+1}(M)$ corresponds to the region with $k^* = n$, i.e., the Fermi level has exactly $n + 1$ bands below it. In Fig. 6, we show the (M, c) plane and some critical lines that demarcates various regions. In each region, we have also sketched a typical/representative density profile. Next, we will discuss the density in the ground state.

Appendix D: Density as a function of space (exact expression for finite N)

We recap (Eq. A22) that the single particle wave functions can be written as

$$\psi_{k,l}(r, \theta) = a_{k,l} L_k^\lambda(r^2) r^\lambda e^{-r^2/2} e^{il\theta}, \quad (D1)$$

with

$$a_{k,l}^2 = \frac{\Gamma(k+1)}{\pi \Gamma(k+1+\lambda)} \text{ and } \lambda = \sqrt{\gamma + l^2}. \quad (D2)$$

$L_k^\alpha(x)$ are the generalized Laguerre polynomials. The average density in the ground state is given by the general formula,

$$\begin{aligned} \rho(r, \theta, N) &= \sum_{k,l} |\psi_{k,l}(r, \theta)|^2 \\ &= \frac{e^{-r^2}}{\pi} \sum_{k=0}^{k^*} \sum_{l=l_-(k)}^{l_+(k)} \frac{\Gamma(k+1) [L_k^\lambda(r^2)]^2 r^{2\lambda}}{\Gamma(\lambda + k + 1)} \\ &= \sum_{k=0}^{k^*} \rho_k(r, \theta, N) \end{aligned} \quad (D3)$$

where $l_\pm(k)$ are given in Eq. B18 with μ determined from Eq. B20. The contribution to the density from the k^{th} band is given by,

$$\rho_k(r, \theta, N) = \frac{\Gamma(k+1) e^{-r^2}}{\pi} \sum_{l=l_-(k)}^{l_+(k)} \frac{[L_k^\lambda(r^2)]^2 r^{2\lambda}}{\Gamma(\lambda + k + 1)} \quad (D4)$$

The above expression for density (Eq. D3 and Eq. D4) is valid for any N (see Fig. 7). In what follows, we will take the large- N limit and provide further analytical insight into the form of the density.

Appendix E: Density as a function of space in the large N limit

In the large N limit, noting that both $l_\pm(k)$ scale as N , we set $l = Ny$ and replace the discrete sum over l by an integral over y . Furthermore, we scale $r = z\sqrt{N}$. With this change of variable, we want to first express the integrand as a function of y for fixed z in the limit of large N . Let us start with the quantity $\lambda = \sqrt{\gamma + l^2}$. Recollecting that $\gamma = cN$ and setting $l = Ny$, we get for large N ,

$$\lambda \simeq Ny + \frac{c}{2y} \quad (E1)$$

Approximating the Gamma function in Eq. D4 by the Stirling formula $\Gamma(z+1) \sim \sqrt{2\pi} e^{(z+\frac{1}{2}) \log(z)} z^z$ for large z and setting $r = z\sqrt{N}$, we find to leading order for large N ,

$$\rho_k(r, \theta, N) \approx \frac{\sqrt{N}\Gamma(k+1)}{\pi\sqrt{2\pi}} \int_{\lambda_-(k)}^{\lambda_+(k)} \frac{dy}{\sqrt{y}} e^{N[y \ln(z^2/y) + y - z^2]} (Ny)^{-k} [L_k^{Ny}(z^2 N)]^2, \quad (\text{E2})$$

where $\lambda_{\pm}(k)$ has been defined in Eq. B18. In the large N limit, the integral over y is dominated by a saddle point at $y = z^2$. Therefore it is natural to make the change of variable,

$$y = z^2 + \sqrt{\frac{2}{N}} x z. \quad (\text{E3})$$

Therefore $Nz^2 \approx Ny - x\sqrt{2Ny}$. We can now use the following remarkable limiting formula for the generalized Laguerre polynomials,

$$\lim_{\lambda \rightarrow \infty} \lambda^{-k/2} L_k^\lambda(\lambda - \sqrt{2\lambda}x) = \frac{2^{-k/2}}{\Gamma(k+1)} H_k(x), \quad (\text{E4})$$

where $H_k(x)$ is the Hermite polynomial of index k . Substituting $\lambda \approx Ny$ and using $Nz^2 \approx Ny - x\sqrt{2Ny}$ we find, using Eq. E4, that,

$$\lim_{N \rightarrow \infty} (Ny)^{-k} [L_k^{Ny}(Ny - x\sqrt{2Ny})]^2 = \frac{2^{-k}}{[\Gamma(k+1)]^2} H_k^2(x). \quad (\text{E5})$$

Thus the integral in Eq. E2 reads

$$\rho_k(r, \theta, N) \approx \frac{2^{-k}}{\pi^{3/2}\Gamma(k+1)} \int_{a_-(k)}^{a_+(k)} dx e^{-x^2} [H_k(x)]^2, \quad (\text{E6})$$

where

$$a_{\pm}(k) = \frac{(\lambda_{\pm}(k) - z^2)\sqrt{N}}{z\sqrt{2}}. \quad (\text{E7})$$

Therefore, the density in the k^{th} band is supported on the interval $\sqrt{\lambda_-(k)} < z < \sqrt{\lambda_+(k)}$. It turns out that this expression for the density has very interesting bulk and edge properties. In the subsequent subsections we analyse these properties.

1. Bulk

If z is in the bulk, i.e. far away from these two edges, then in the large N limit, the two limits $a_{\pm}(k) \rightarrow \pm\infty$. Hence the integral becomes simply $\int_{-\infty}^{\infty} du e^{-u^2} [H_k(u)]^2 = 2^k \Gamma(k+1) \sqrt{\pi}$. This gives the bulk density,

$$\rho_k^{\text{bulk}}(r, \theta, N) \approx \frac{1}{\pi} \mathcal{I}_{\sqrt{\lambda_-(k)} < z < \sqrt{\lambda_+(k)}} \quad (\text{E8})$$

where $\mathcal{I}_{\sqrt{\lambda_-(k)} < z < \sqrt{\lambda_+(k)}}$ is an indicator function that takes value 1 if the inequality in the subscript is satisfied and 0 otherwise.

Let us summarise the results of above Sec E1. The total density is obtained by summing over all the bands below the Fermi energy and is given by its large N scaling form,

$$\rho(r, \theta, N) \sim f\left(\frac{r}{\sqrt{N}}\right), \quad (\text{E9})$$

where the scaling function $f(z)$ is given by,

$$f(z) = \frac{1}{\pi} \sum_{k=0}^{k^*} \mathcal{I}_{\sqrt{\lambda_-(k)} < z < \sqrt{\lambda_+(k)}}, \quad (\text{E10})$$

and $\lambda_{\pm}(k)$ is given in Eq. B18. One can check that $f(z)$ in Eq. E10 is normalized, i.e. $2\pi \int_0^\infty f(z) z dz = 1$ upon using the definition of $\lambda_{\pm}(k)$ from Eq. B18 and the relation in Eq. B20.

Hence the limiting density has a compact single support over $\sqrt{\lambda_-(0)} < z < \sqrt{\lambda_+(0)}$. For $k^* = 0$, it is just a simple flat density over this support. However, for $k^* > 0$, the density has a nontrivial layered shape. For example, for $k^* = 1$, the density is given by (see Fig. 7),

$$f(z) = \begin{cases} 0, & z < \sqrt{\lambda_-(0)} \\ \frac{1}{\pi}, & \sqrt{\lambda_-(0)} < z < \sqrt{\lambda_-(1)} \\ \frac{2}{\pi}, & \sqrt{\lambda_-(1)} < z < \sqrt{\lambda_+(1)} \\ \frac{1}{\pi}, & \sqrt{\lambda_+(1)} < z < \sqrt{\lambda_+(0)} \\ 0, & z > \sqrt{\lambda_+(0)}. \end{cases} \quad (\text{E11})$$

2. Edges

In contrast if z is close to one of the two edges, say the left edge $\sqrt{\lambda_-(k)}$, we can estimate the limiting form of the edge density when $N \rightarrow \infty$ from the same expression in Eq. E6. For this, we set,

$$z^2 = \lambda_-(k) + \frac{\sqrt{2\lambda_-(k)}}{\sqrt{N}} u, \quad (\text{E12})$$

where $u \sim O(1)$. In this case, the lower limit in the integral in Eq. E6 becomes $a_-(k) \approx -u$ (with u measuring the scaled distance from the left edge), while the upper limit still approaches to $+\infty$ as $N \rightarrow \infty$. Hence we get,

$$\rho_k^{\text{edge}}(r, \theta, N) \rightarrow f_k^{\text{edge}}(u) \quad (\text{E13})$$

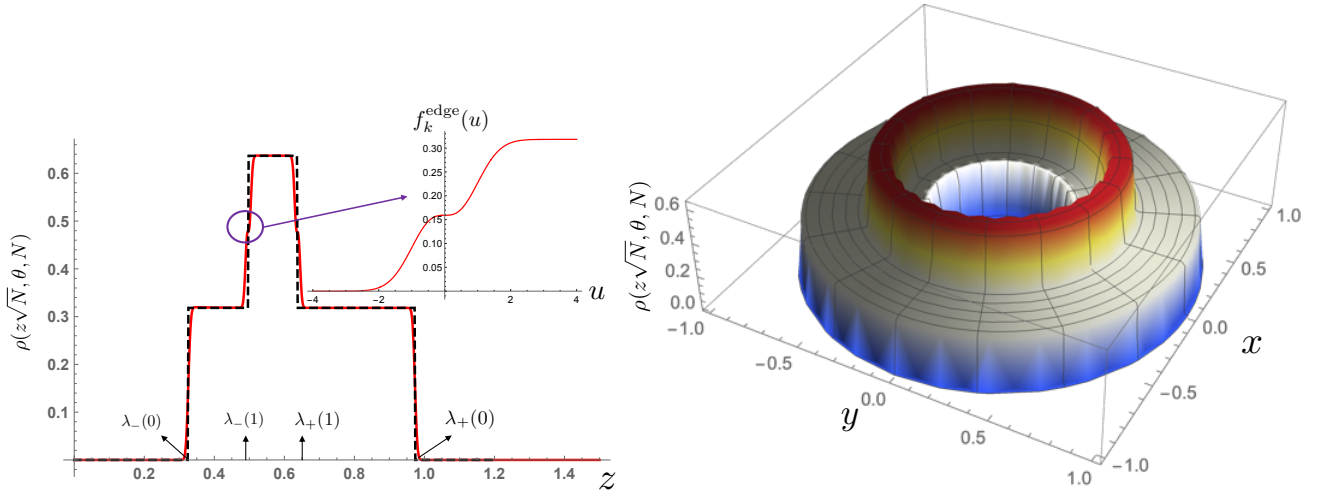


FIG. 7. (Left) Plot showing the comparison between exact expression for density (Eq. D3, red solid) and the bulk density expression at large- N (Eq. E8, black dashed). We chose, $c = 1$, $M = 10$ and $N = 8000$ and we are in the $k^* = 1$ region of Fig. 6. We also notice the two kinks (red solid) which stems from the zeros of Hermite Polynomial of degree $k = 1$ in our case. We have zoomed the location of the kink for the left edge and shown $f_1^{\text{edge}}(u)$. (Right) A three-dimensional representation of exact expression for density (Eq. D3). We can see the non-trivial layered structure ($z = \sqrt{x^2 + y^2}$).

where

$$f_k^{\text{edge}}(u) = \frac{2^{-k}}{\pi^{3/2}\Gamma(k+1)} \int_{-u}^{\infty} dx e^{-x^2} [H_k(x)]^2 \quad (\text{E14})$$

and we recall that,

$$u = \sqrt{\frac{N}{2\lambda_-(k)}} \left(\frac{r^2}{N} - \lambda_-(k) \right). \quad (\text{E15})$$

Note that when $u \rightarrow \infty$, $f_k^{\text{edge}}(u) \rightarrow 1/\pi$, and the edge density matches smoothly with the bulk density. In Fig. 8 we have plotted the edge density functions $f_k^{\text{edge}}(u)$ vs u for $k = 1$ and $k = 2$. One sees from these figures that the scaling functions have kinks. For $k = 1$, there is only one kink at $u = 0$ while for $k = 2$ there are two kinks. In general, for the k^{th} band, the function $f_k(u)$ will have k kinks as a function of u . The kinks occur when the derivative vanishes, i.e., $df_k^{\text{edge}}(u)/du = 0$. By taking the derivative of Eq. E13, we see that this

happens when $H_k(-u) = 0$. Thus the locations of the kinks in the edge density of the k^{th} band coincide with the zeroes of the k^{th} Hermite polynomial. For instance, for $k = 2$, the kinks are located at $u_1 = -1/\sqrt{2}$ and $u_2 = +1/\sqrt{2}$. Note that the edge scaling function $f_k(u)$ is actually universal, i.e. independent of the system parameters c and M and depends only on the band label k . The above non-trivial connection between $f_k^{\text{edge}}(u)$ and Hermite polynomials naturally points to a possible connection to RMT, which we elucidate below.

3. Edge density in the limit of high Landau levels ($k \gg 1$) and connection to Random Matrix Theory

It turns out that as $k \rightarrow \infty$, the edge profile $f_k^{\text{edge}}(u)$ given in Eq. E13, property shifted and scaled, has a nice limiting profile. This behaviour comes from the asymptotic behavior of the Hermite polynomials $H_k(u)$ in the limit of large k (known as Plancherel-Rotach asymptotics). To obtain this limiting profile, we first set $u = \sqrt{2k}y$, with $y \sim O(1)$, and also perform the change of variable in Eq. E13, $x = \sqrt{2k}(v - y)$. This leads to,

$$f_k^{\text{edge}}(u = \sqrt{2k}y) = \frac{2^{-k}\sqrt{2k}}{\pi^{3/2}\Gamma(k+1)} \int_0^{\infty} dv \left[e^{-k(v-y)^2} H_k(\sqrt{2k}(v-y)) \right]^2. \quad (\text{E16})$$

We can now use the Plancherel-Rotach asymptotic formula for Hermite polynomials,

$$e^{-kX^2} H_k(\sqrt{2k}X) = \left(\frac{2}{\pi} \right)^{1/4} \frac{2^{k/2}}{(1-X^2)^{1/4}} k^{-1/4} (k!)^{1/2} \times g_k(X) \left(1 + \mathcal{O}\left(\frac{1}{k}\right) \right), \quad -1 < X < 1 \quad (\text{E17})$$

with

$$g_k(X) = \cos \left(kX\sqrt{1-X^2} + (k+1/2)\sin^{-1}X - k\pi/2 \right) \quad (\text{E18})$$

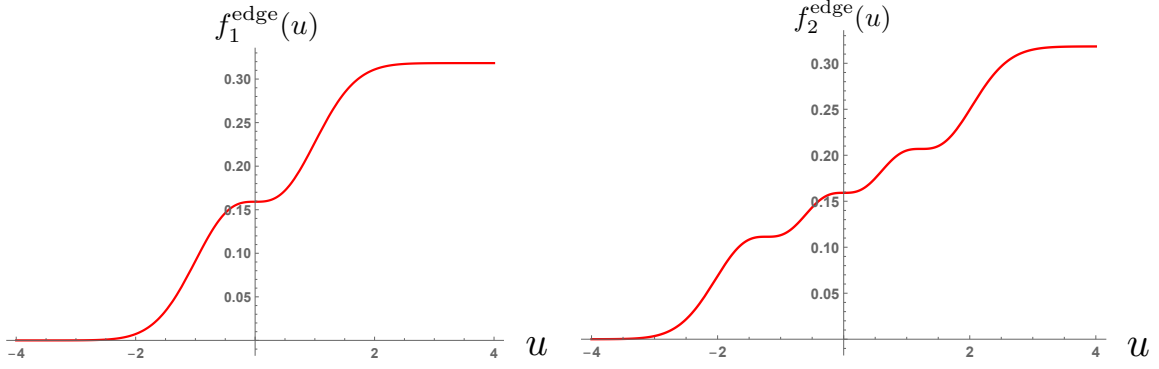


FIG. 8. The edge density scaling functions $f_k^{\text{edge}}(u)$, i.e., Eq. E13 is plotted vs u for $k = 1$ (left panel) and $k = 2$ (right panel). We see that the location of the kinks is at $H_k(u) = 0$.

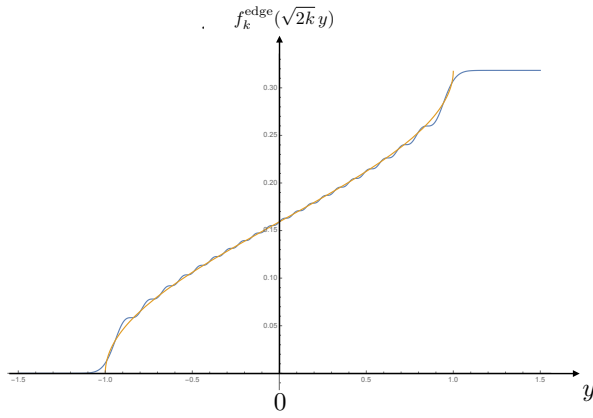


FIG. 9. Plot of $f_k^{\text{edge}}(\sqrt{2k}y)$, with $f_k^{\text{edge}}(y)$ given in Eq. E13 as a function of y for $k = 20$ (red solid line). The black-dashed line is the exact limiting form given in Eq. E21. It should be noted that the positions of kinks are at zeros of Hermite polynomial of degree $k = 20$.

Inserting this expansion (Eq. E17 and Eq. E18) with

$X = v - y$ in Eq. E16, one finds,

$$f_k^{\text{edge}}(u = \sqrt{2k}y) \approx \frac{2}{\pi^2} \int_0^\infty \mathcal{I}_{-1 < v-y < 1} \times \frac{1}{\sqrt{1-(v-y)^2}} g_k^2(v-y) dv \quad (\text{E19})$$

where the indicator function comes from the fact that the asymptotic behavior in Eq. E17 and Eq. E18 holds only for $-1 < X < 1$, while it is sub-leading (in k) for X outside the region. Due to the identity $\cos^2 x = 1/2 + \cos(2x)/2$, one can replace $[g_k(v-y)]^2$, given in Eq. E18, in the integral over v in Eq. E19 by $1/2$ (the remaining cosine being highly oscillating for large k and thus subleading). Therefore we get,

$$f_k^{\text{edge}}(u = \sqrt{2k}y) \approx \frac{1}{\pi^2} \int_{\max(y-1,0)}^{\max(y+1,0)} \frac{dv}{\sqrt{1-(v-y)^2}} \quad (\text{E20})$$

which finally yields (see also Fig. 9),

$$\lim_{k \rightarrow \infty} f_k^{\text{edge}}(u = \sqrt{2k}y) = \begin{cases} 0, & y < -1 \\ \frac{1}{\pi^2} \left(\frac{\pi}{2} + \sin^{-1}(y) \right), & -1 < y < 1 \\ \frac{1}{\pi}, & y > 1. \end{cases} \quad (\text{E21})$$

Close to $u = \pm\sqrt{2k}$ there is an interesting edge region, of width $O(k^{-1/6})$ where the density is described by Airy functions, very similar to the well known ‘‘Tracy-Widom’’ regime at the edge of the Wigner semi-circle in RMT belonging to the Gaussian Unitary Ensemble (GUE). This is somehow expected given the square-root singularity near the edges $u = \pm\sqrt{2k}$ of the limiting profile given in

Eq. E21. This edge behavior can be derived from Eq. E13 by using the asymptotic behavior of the Hermite polynomial $H_k(u)$ near $u = \sqrt{2k}$ where the Hermite polynomial becomes an Airy function. One finds (for large k), setting

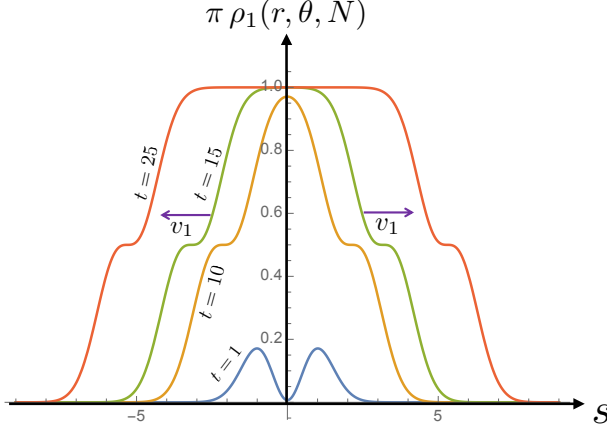


FIG. 10. Plot of the density profile $\pi\rho_1(r, \theta, N)$ as given in Eq. F17 for $M = 5$, as a function of the scaled distance s – we recall that $r = z\sqrt{N} \approx \sqrt{N}(c_1/M)^{1/4} + s/\sqrt{2}$ – for different increasing values of $t = 1, 10, 15$ and 25 (from bottom to top). As t increases, the scaled density $\pi\rho_1(r, \theta, N)$ approaches the constant value 1 for $|s| < v_1 t$ and decays rapidly to 0 for $|s| > v_1 t$. The front separating the constant density $1/\pi$ and the zero-density outside “moves with a constant speed v_1 ” with increasing t , reminiscent of a remarkable travelling front structure.

$$u = -\sqrt{2k} + \frac{w}{\sqrt{2k^{1/6}}} \text{ with } w = O(1)$$

$$f_k \left(-\sqrt{2k} + \frac{w}{\sqrt{2k^{1/6}}} \right) \sim \frac{1}{k^{1/3}} \mathcal{F}(w) \quad (\text{E22})$$

where

$$\mathcal{F}(w) = \frac{1}{\pi} \int_0^\infty \text{Ai}^2(v-w) dv = \frac{1}{\pi} ([\text{Ai}'(-w)]^2 + w \text{Ai}^2(-w)) \quad (\text{E23})$$

and $\text{Ai}(z)$ denotes the standard Airy function. Note that a similar computation could be carried out for the kernel which would lead (on the real line at least) to the well known Airy kernel.

Appendix F: Emergence of new droplet as one crosses critical lines in (M, c) plane

We want to look at the phase diagram in the (M, c) plane and ask, when k^* changes from $k^* = 0$ to $k^* = 1$ (which means a new band is included below the Fermi energy), how does the density profile change from one layered structure to two layered structure. We have already seen that just when one crosses this critical line $c = c_1(M) \equiv c_1$, the second layer appears on top of the first layer. In this subsection, we describe the density profile of this emerging blob in the second layer for c slightly below c_1 for fixed $4 < M < 12$ (see Fig. 6), where c_1 is given in Eq. C2. We therefore set

$$c = c_1 - \Delta \text{ where } 0 < \Delta \ll 1. \quad (\text{F1})$$

For each point in the (M, c) plane, μ is uniquely determined from Eq. B20. Therefore as we change the value of c from c_1 to $c_1 - \Delta$, the value of μ also changes from $\mu = 2 + \sqrt{c_1 M}$ to

$$\mu = 2 + \sqrt{c_1 M} + \delta, \quad (\text{F2})$$

where $\delta \ll 1$. Inserting this value of μ in Eq. B20 and expanding for small δ gives a relation between Δ and δ

$$\Delta = \frac{(M^2 - 16)^{3/2}}{64\sqrt{2}} \sqrt{\delta}. \quad (\text{F3})$$

Therefore, one just has one single control parameter δ describing the location of the system in the phase diagram, in the vicinity of the critical line $c = c_1(M)$. We now want to see how the density changes as we vary δ .

We start with the formula for the density in Eq. D3. When k^* increases from 0 to 1 , the additional density in the second layer is given by,

$$\rho_1(r, \theta, N) = \frac{e^{-r^2}}{\pi} \sum_{l=l_-(1)}^{l_+(1)} \frac{r^2 \sqrt{\gamma + l^2}}{\Gamma(\sqrt{\gamma + l^2} + 2)} \left[L_1^{\sqrt{\gamma + l^2}}(r^2) \right]^2 \quad (\text{F4})$$

with

$$L_1^{\sqrt{\gamma + l^2}}(r^2) = 1 + \sqrt{\gamma + l^2} - r^2 \quad (\text{F5})$$

where,

$$l_{\pm}(1) = \frac{\mu - 2 \pm \sqrt{(\mu - 2)^2 - c_1 M}}{M} N. \quad (\text{F6})$$

We can rewrite Eq. F6 using Eq. F2 (to leading order in δ for small δ) as,

$$l_{\pm}(1) \approx \lambda_{\pm} N, \quad \lambda_{\pm} = \left(\sqrt{\frac{c_1}{M}} \pm v_1 \sqrt{\delta} \right) \quad (\text{F7})$$

with

$$v_1 = \frac{\sqrt{2}}{M} (c_1 M)^{1/4}. \quad (\text{F8})$$

In real space, the second layer of the macroscopic density appears over the scaled region,

$$\sqrt{\frac{c_1}{M}} - v_1 \sqrt{\delta} < z^2 < \sqrt{\frac{c_1}{M}} + v_1 \sqrt{\delta}, \quad (\text{F9})$$

where $z = r/\sqrt{N}$. Therefore, the center of the second layer is located at $z_c = (c_1/M)^{1/4}$ and we want to provide a scaling description of this density in the second layer just after its appearance, i.e., in the limit $\delta \rightarrow 0$. Hence we set,

$$z^2 = \sqrt{\frac{c_1}{M}} + \epsilon, \quad (\text{F10})$$

where ϵ is proportional to the distance from the center of the second layer. Thus the density is just a function of ϵ and δ in the vicinity of the critical line $c = c_1(M)$

and below we work out the dependence of the density on these two parameters in the large N limit.

To analyse the density Eq. F4 in the limit of large N ,

$$\rho_1(r, \theta, N) \approx \frac{e^{-r^2}}{\pi} \int_{\lambda_-}^{\lambda_+} dx \frac{r^{2\sqrt{cN+N^2x^2}}}{\Gamma(\sqrt{cN+N^2x^2}+2)} \left[1 + \sqrt{cN+N^2x^2} - r^2\right]^2 \approx \frac{e^{-r^2}}{\pi} \int_{\lambda_-}^{\lambda_+} dx \frac{r^{2Nx}}{\Gamma(Nx+2)} (Nx - r^2)^2 \quad (\text{F11})$$

where we kept the leading term in the arguments for large

we set $\gamma = c_1 N$ and we introduce $l = xN$ so that the sum over l can be replaced by an integral over x leading to,

N . We can now approximate the Gamma function by the Stirling's formula, leading to,

$$\rho_1(r = z\sqrt{N}, \theta, N) \approx \frac{e^{-Nz^2}}{\pi\sqrt{2\pi N}} \int_{\lambda_-}^{\lambda_+} \frac{dx}{x^{3/2}} e^{2Nx \ln(z\sqrt{N}) - Nx \ln x + Nx} (Nx - Nz^2)^2. \quad (\text{F12})$$

We now substitute $z^2 = \sqrt{c_1/M} + \epsilon$ from Eq. F10 and make the change of variable $x = \sqrt{c_1/M} + v$. Since $|v| <$

$v_1\sqrt{\delta}$, we can expand the integrand for small v and retain only up to $O(v^2)$ terms inside the exponential. After straightforward algebra, one obtains,

$$\rho_1(r = z\sqrt{N}, \theta, N) \approx \frac{1}{\pi\sqrt{2\pi N}} \left(\frac{M}{c_1}\right)^{3/4} \int_{-v_1\sqrt{\delta}}^{+v_1\sqrt{\delta}} dv e^{-N\sqrt{\frac{M}{4c_1}}(v-\epsilon)^2} N^2(v-\epsilon)^2. \quad (\text{F13})$$

In order that this integral is of order $O(1)$, we see that we need to scale $\sqrt{\delta} \sim t/\sqrt{N}$, $\epsilon \sim s/\sqrt{N}$ where $t > 0$ as well as s are both of order $O(1)$. Making the change of variable $\tilde{w} = [N/2]^{1/2}(M/c_1)^{1/4}(v-\epsilon)$ in Eq. F13, we get,

$$\rho_1(r = z\sqrt{N}, \theta, N) \approx \frac{2}{N} \frac{1}{\pi^{3/2}} \int_{\tilde{w}_-}^{\tilde{w}_+} d\tilde{w} \tilde{w}^2 e^{-\tilde{w}^2} \quad (\text{F14})$$

with

$$\tilde{w}_{\pm} = \sqrt{\frac{N}{2}} \left(\frac{M}{c_1}\right)^{1/4} (\pm v_1\sqrt{\delta} - \epsilon). \quad (\text{F15})$$

In order that the integral remains of order $O(1)$ in the large N limit, we see that both $\sqrt{\delta}$ and ϵ should scale as $O(1/\sqrt{N})$. We therefore set,

$$\sqrt{\delta} = \sqrt{\frac{2}{N}} \left(\frac{c_1}{M}\right)^{1/4} t \quad \text{and} \quad \epsilon = \sqrt{\frac{2}{N}} \left(\frac{c_1}{M}\right)^{1/4} s, \quad (\text{F16})$$

where t and s are both of order $O(1)$. Therefore, the density in the large N limit, a function of the original variables ϵ and δ , can be re-paramaterized in terms of

the scaled variables s and t given in Eq. F16

$$\rho_1(r = z\sqrt{N}, \theta, N) \approx \frac{1}{\pi} [F_1(s + v_1 t) - F_1(s - v_1 t)], \quad (\text{F17})$$

where $v_1 = \frac{\sqrt{2}}{M}(c_1 M)^{1/4}$ and

$$F_1(z) = \frac{2}{\sqrt{\pi}} \int_0^z d\tilde{w} \tilde{w}^2 e^{-\tilde{w}^2} = \frac{1}{2} \left[\text{erf}(z) - \frac{2}{\sqrt{\pi}} z e^{-z^2} \right]. \quad (\text{F18})$$

Note that the scaled variables t and s can be expressed in terms of $\Delta = c_1 - c$ (which measures the location the distance in the phase diagram with respect to the critical line $c = c_1(M)$) and the variable $z = r/\sqrt{N}$ where r measures the distance from the center of the trap. The first relation can be obtained by eliminating δ between Eqs. F3 and F16

$$t = \left(\frac{M}{4c_1}\right)^{1/4} \frac{64\sqrt{2}}{(M^2 - 16)^{3/2}} [c_1 - c] \sqrt{N}. \quad (\text{F19})$$

Similarly the second relation is obtained by substituting $\epsilon = z^2 - \sqrt{c_1/M}$ in Eq. F16. This gives

$$s = \left(\frac{M}{4c_1}\right)^{1/4} \left(z^2 - \frac{c_1}{M}\right) \sqrt{N}, \quad (\text{F20})$$

where $z = r/\sqrt{N}$.

Interestingly, the scaled density profile in Eq. F17 has an interesting traveling front structure. To see this, we consider the density as a function of s , for a fixed t . The density decays to 0 very rapidly as $|s| \gg v_1 t$ (see Fig. 10). Therefore the two edges of this profile move “ballistically” with increasing t with a “speed” given by v_1 . If we interpret t as a “time”, then at late times, the density profile develops a traveling front structure with velocity v_1 and the width across the front remains of $O(1)$ as t increases. For large t , the density has a constant value $\simeq 1/\pi$ for all $|s| < v_1 t$ (see Fig. 10). Finally, the speed v_1 is given by $v_1 = \sqrt{2/M(c_1 M)^{1/4}}$ can be expressed in terms of M , by using the expression for $c_1(M)$ in Eq. C2.

Note that here we analysed the density profile near the transition from $k^* = 0$ to $k^* = 1$ where the second layer

just appears over the first layer. One can do a similar analysis for the transition form $k^* = n - 1$ to $k^* = n$ across the critical line $c = c_n(M)$ for any $n \geq 1$. We do not repeat the analysis here but it is easy to show that the scaled density will again be given by the difference of two functions, as in the $k = 1$ case in Eq. F17,

$$\rho_n(r = z\sqrt{N}) \approx \frac{1}{\pi} [F_n(s + v_n t) - F_n(s - v_n t)] \quad (\text{F21})$$

where the speed v_n can be computed from the critical curve $c = c_n(M)$ and the scaling function $F_n(z)$ is given, up to an overall constant by,

$$F_n(z) \propto \int_0^z d\tilde{w} [H_n(\tilde{w})]^2 e^{-\tilde{w}^2}, \quad (\text{F22})$$

where $H_n(\tilde{w})$ is the Hermite polynomial of degree n .

-
- [1] I. Bloch, J. Dalibard, and W. Zwerger, *Rev. Mod. Phys.*, **80**, 885 (2008).
 - [2] S. Nascimbene, N. Navon, F. Chevy, and C. Salomon, *New J. Phys.*, **12**, 103026 (2010).
 - [3] L. W. Cheuk, M. A. Nichols, M. Okan, T. Gersdorf, V. V. Ramasesh, W. S. Bakr, T. Lompe, and M. W. Zwierlein, *Phys. Rev. Lett.*, **114**, 193001 (2015).
 - [4] E. Haller, J. Hudson, A. Kelly, D. A. Cotta, B. Peaudecerf, G. D. Bruce, and S. Kuhr, *Nature Physics*, **11**, 738 (2015).
 - [5] M. F. Parsons, F. Huber, A. Mazurenko, C. S. Chiu, W. Setiawan, K. Wooley-Brown, S. Blatt, and M. Greiner, *Phys. Rev. Lett.*, **114**, 213002 (2015).
 - [6] B. Mukherjee, Z. Yan, P. B. Patel, Z. Hadzibabic, T. Yefsah, J. Struck, and M. W. Zwierlein, *Phys. Rev. Lett.*, **118**, 123401 (2017).
 - [7] K. Hueck, N. Luick, L. Sobirey, J. Siegl, T. Lompe, and H. Moritz, *Phys. Rev. Lett.*, **120**, 060402 (2018).
 - [8] M. Inguscio, W. Ketterle, and C. Salomon, *Ultra-cold Fermi gases*, Vol. 164 (IOS press, 2008).
 - [9] S. Giorgini, L. P. Pitaevskii, and S. Stringari, *Rev. Mod. Phys.*, **80**, 1215 (2008).
 - [10] J. Joseph, J. E. Thomas, M. Kulkarni, and A. G. Abanov, *Phys. Rev. Lett.*, **106**, 150401 (2011).
 - [11] L. W. Cheuk, M. A. Nichols, M. Okan, T. Gersdorf, V. V. Ramasesh, W. S. Bakr, T. Lompe, and M. W. Zwierlein, *Phys. Rev. Lett.*, **114**, 193001 (2015).
 - [12] E. Haller, J. Hudson, A. Kelly, D. A. Cotta, B. Peaudecerf, G. D. Bruce, and S. Kuhr, *Nature Physics*, **11**, 738 (2015).
 - [13] M. F. Parsons, F. Huber, A. Mazurenko, C. S. Chiu, W. Setiawan, K. Wooley-Brown, S. Blatt, and M. Greiner, *Phys. Rev. Lett.*, **114**, 213002 (2015).
 - [14] E. Vicari, *Phys. Rev. A*, **85**, 062104 (2012).
 - [15] V. Eisler, *Phys. Rev. Lett.*, **111**, 080402 (2013).
 - [16] R. Marino, S. N. Majumdar, G. Schehr, and P. Vivo, *Phys. Rev. Lett.*, **112**, 254101 (2014).
 - [17] D. S. Dean, P. Le Doussal, S. N. Majumdar, and G. Schehr, *Phys. Rev. Lett.*, **114**, 110402 (2015).
 - [18] D. S. Dean, P. Le Doussal, S. N. Majumdar, and G. Schehr, *EPL*, **112**, 60001 (2015).
 - [19] D. S. Dean, P. Le Doussal, S. N. Majumdar, and G. Schehr, *Phys. Rev. A*, **94**, 063622 (2016).
 - [20] R. Marino, S. N. Majumdar, G. Schehr, and P. Vivo, *Phys. Rev. E*, **94**, 032115 (2016).
 - [21] D. Butts and D. Rokhsar, *Phys. Rev. A*, **55**, 4346 (1997).
 - [22] W. Kohn and A. E. Mattsson, *Phys. Rev. Lett.*, **81**, 3487 (1998).
 - [23] D. S. Dean, P. Le Doussal, S. N. Majumdar, and G. Schehr, *J. Phys. A: Math. Theor.*, **52**, 144006 (2019).
 - [24] P. Calabrese, P. Le Doussal, and S. N. Majumdar, *Phys. Rev. A*, **91**, 012303 (2015).
 - [25] B. Lacroix-A-Chez-Toine, P. Le Doussal, S. N. Majumdar, and G. Schehr, *EPL*, **120**, 10006 (2017).
 - [26] D. S. Dean, P. Le Doussal, S. N. Majumdar, and G. Schehr, *Phys. Rev. A*, **97**, 063614 (2018).
 - [27] P. Le Doussal, S. N. Majumdar, and G. Schehr, *Phys. Rev. Lett.*, **121**, 030603 (2018).
 - [28] F. D. Cunden, S. N. Majumdar, and N. O’Connell, *J. Phys. A: Math. Theor.*, **52**, 165202 (2019).
 - [29] T.-L. Ho and C. Ciobanu, *Phys. Rev. Lett.*, **85**, 4648 (2000).
 - [30] A. Aftalion, X. Blanc, and J. Dalibard, *Phys. Rev. A*, **71**, 023611 (2005).
 - [31] V. Schweikhard, I. Coddington, P. Engels, V. Mogenendorff, and E. A. Cornell, *Phys. Rev. Lett.*, **92**, 040404 (2004).
 - [32] A. L. Fetter, *Rev. Mod. Phys.*, **81**, 647 (2009).
 - [33] N. R. Cooper, *Adv. Phys.*, **57**, 539 (2008).
 - [34] B. Lacroix-A-Chez-Toine, S. N. Majumdar, and G. Schehr, *Phys. Rev. A*, **99**, 021602 (2019).
 - [35] L. D. Landau, E. M. Lifšic, E. M. Lifshitz, and L. Pitaevskii, *Statistical physics: theory of the condensed state*, Vol. 9 (Butterworth-Heinemann, 1980).
 - [36] A. J. Leggett *et al.*, *Quantum liquids: Bose condensation and Cooper pairing in condensed-matter systems* (Oxford university press, 2006).
 - [37] N. R. Cooper, *Many-Body Physics with Ultracold Gases: Lecture Notes of the Les Houches Summer School: Volume 94, July 2010*, **94**, 189 (2012).
 - [38] P. J. Forrester, *Log-gases and random matrices (LMS-34)* (Princeton University Press, 2010).
 - [39] T. Antal, Z. Rácz, A. Rákos, and G. M. Schütz, *Physical Review E*, **59**, 4912 (1999).

- [40] T. Antal, P. L. Krapivsky, and A. Rákos, Phys. Rev. E, **78**, 061115 (2008).
- [41] V. Eisler and Z. Rácz, Phys. Rev. Lett., **110**, 060602 (2013).
- [42] V. Hunyadi, Z. Rácz, and L. Sasvári, Phys. Rev. E, **69**, 066103 (2004).
- [43] B. Mukherjee, K. Sengupta, and S. N. Majumdar, Phys. Rev. B, **98**, 104309 (2018).
- [44] M. Kulkarni, S. N. Majumdar, and G. Schehr, Supplementary Material.
- [45] G. V. Dunne, Int. J. Mod. Phys. B, **8**, 1625 (1994).
- [46] A. Haimi and H. Hedenmalm, J. Stat. Phys., **153**, 10 (2013).
- [47] M. J. Bowick and É. Brézin, Phys. Lett. B, **268**, 21 (1991).
- [48] P. J. Forrester, Nucl. Phys. B, **402**, 709 (1993).
- [49] We recall that the relation between r and s reads $r = z\sqrt{N} \approx (c_1/M)^{1/4}\sqrt{N} + s/\sqrt{2}$ for large N .
- [50] I. D. Rodríguez and G. Sierra, Phys. Rev. B, **80**, 153303 (2009).
- [51] L. Charles and B. Estienne, Commun. Math. Phys., **376**, 521 (2019).
- [52] H. Leschke, A. V. Sobolev, and W. Spitzer, arXiv preprint arXiv:2007.06316 (2020).
- [53] P. C. Haljan, I. Coddington, P. Engels, E. A. Cornell, Phys. Rev. Lett. **87**, 210403 (2001).
- [54] M. W. Zwierlein, J. R. Abo-Shaeer, A. Schirotzek, C. H. Schunck, W. Ketterle, Nature **435**, 1047 (2005).
- [55] S. Gradshteyn and I. M. Ryzhik, Table of integrals, series, and products (Academic press, 2014).